Comparison of 3T and 7T ASL techniques for concurrent functional perfusion and BOLD studies

NeuroImage 156 (2017) 363–376

Contents lists available at ScienceDirect

NeuroImage

journal homepage: www.elsevier.com/locate/neuroimage

Comparison of 3 T and 7 T ASL techniques for concurrent functional perfusion and BOLD studies

Dimo Ivanov[a,*,1], Anna Gardumi[a,1], Roy A.M. Haast[a], Josef Pfeuffer[b], Benedikt A. Poser[a], Kâmil Uludağ[a]

[a] Department of Cognitive Neuroscience, Faculty of Psychology and Neuroscience, Maastricht University, Maastricht, The Netherlands
[b] Siemens Healthcare, MR Application Development, Erlangen, Germany

ARTICLE INFO

Keywords:
Arterial spin labeling
Cerebral blood flow
BOLD signal
Functional imaging
Ultra-high field
Parallel imaging
Dual-echo

ABSTRACT

Arterial spin labeling (ASL) is the primary non-invasive MRI approach to measure baseline cerebral blood flow (CBF) in healthy subjects and patients. ASL also allows concurrent functional BOLD signal and CBF measurements, but the latter typically suffer from low contrast-to-noise (CNR) ratio. Ultra-high-field imaging significantly boosts BOLD signal CNR. However, it is contested whether also CBF CNR benefits from increasing magnetic field strength, especially given that technical challenges related to field inhomogeneities and power deposition constraints exist. Recently, we presented an optimized PASL technique that utilizes tr-FOCI inversion pulses and dielectric pads to overcome the temporal resolution limitations of previous 7 T ASL implementations (Ivanov et al., in press; 2017). The primary goal of this study was to compare its performance to that of 3 T ASL approaches – both pulsed ASL (PASL) and pseudo-continuous (pCASL) – concerning functional studies using simultaneous CBF and BOLD signal acquisition. To this aim, we investigated a wide range of parameters that can influence CBF and BOLD signal sensitivities: spatial resolution, labeling scheme, parallel imaging and echo time. We found that 7 T ASL is superior in terms of CBF and BOLD temporal signal-to-noise ratio (SNR) and activation volume compared to all 3 T ASL variants, in particular at high spatial resolution. Our results show that the advantages of 7 T for ASL stem from increased image SNR, especially when parallel imaging is used. The gray matter baseline CBF was in good agreement for all 3 T ASL variants, but a significantly lower value was obtained at 7 T. The labeling scheme utilized was also found to significantly influence the measured perfusion territories CBF. In conclusion, a single-echo accelerated 7 T PASL is recommended for high spatial and temporal resolution CBF and BOLD imaging, while a 3 T dual-echo pCASL approach without parallel imaging may be preferred for low (i.e., 3 mm isotropic and lower) resolution functional perfusion and BOLD applications.

Introduction

Cerebral blood flow (CBF) can be measured and quantified using arterial spin labeling (ASL) – a non-invasive MRI method, which employs magnetically labeled arterial blood water as an endogenous tracer (Detre et al., 1992; Williams et al., 1992). ASL time-series consist of pairs of label (or tag) and control (i.e., non-labeled) images, whose subtraction produces a signal proportional to the local tissue perfusion while their average represents the BOLD signal (Luh et al., 2000). The non-invasive nature of ASL and its ability to dynamically and quantitatively measure CBF make it an attractive approach for both neuroscience research and clinical applications (Detre et al., 1998;

Abbreviations: ASL, arterial spin labeling; CBF, cerebral blood flow; BOLD, blood oxygenation level-dependent; CNR, contrast-to-noise ratio; tr-FOCI, time-resampled frequency offset corrected inversion; PASL, pulsed ASL; pCASL, pseudo-continuous ASL; fMRI, functional magnetic resonance imaging; SNR, signal-to-noise ratio; PLD, post-labeling delay; UHF, ultra-high field; SAR, specific absorption rate; tSNR, temporal SNR; FAIR, flow-sensitive alternating inversion recovery; PICORE, proximal inversion with a control for off-resonance effects; QUIPSS, quantitative imaging of perfusion using a single subtraction; Q2TIPS, QUIPSS II with thin-slice TI1 periodic saturation; GRAPPA, generalized autocalibrating partially parallel acquisition; EPI, echo planar imaging; MPRAGE, magnetization prepared rapid acquisition gradient echo; FLEET, fast low-angle excitation echo-planar technique; ANOVA, analysis of variance; VC, visual cortex; ACA, anterior cerebral artery; MCA, middle cerebral artery; PCA, posterior cerebral artery; CSF, cerebrospinal fluid; GE, gradient-echo; SE, spin-echo; TFL, turbo fast low angle shot; GM, gray matter; ROI, region of interest; TE, echo time; TI, inversion time; TR, repetition time

* Correspondence to: Dimo Ivanov, Department of Cognitive Neuroscience, Faculty of Psychology & Neuroscience, Maastricht University, PO Box 616, 6200 MD Maastricht, The Netherlands.
E-mail address: dimo.ivanov@maastrichtuniversity.nl (D. Ivanov).
[1] Contributed equally to the work.

http://dx.doi.org/10.1016/j.neuroimage.2017.05.038
Received 29 November 2016; Accepted 17 May 2017
Available online 19 May 2017
1053-8119/

Detre and Wang, 2002). Baseline CBF has been used to study longitudinal intra-subject changes due to, for example, learning, experience and plasticity, and also to examine inter-subject differences in baseline brain physiology in healthy subjects and patients (Detre and Wang, 2002; Krieger et al., 2014). Functional ASL changes have been shown to be better localized to the site of neural activation than the BOLD signal and quantitatively more directly related to neuronal activity (Duong et al., 2001; Tjandra et al., 2005; Cavusoglu et al., 2012; Havlicek et al., 2015). In addition, the capability of ASL to concurrently measure CBF and BOLD signal has proven to be useful for investigating the brain's physiology in health and disease (Bulte et al., 2012; Buxton et al., 2014).

Nevertheless, compared to BOLD fMRI, CBF measurements using ASL present some drawbacks (Alsop et al., 2015), such as: 1) lower signal-to-noise ratio (SNR) of the perfusion-weighted signal due to the low microvascular density (~1–2% of local tissue volume); 2) reduced temporal resolution due to the necessity of a post-labeling delay (PLD) to allow the labeled blood to reach the imaging slab and due to the need to acquire pairs of label and control images; 3) limited brain coverage due to T_1 relaxation of the labeled blood; and 4) increased power deposition.

To overcome these limitations, different ASL approaches have been proposed. An exhaustive overview on how to tackle these limitations, together with protocol recommendations, is given in the ASL white paper (Alsop et al., 2015). In particular, the pseudo-continuous ASL (pCASL) method (Wu et al., 2007; Dai et al., 2008) allows prolonged labeling durations, thus raising SNR, while the use of background suppression improves SNR by reducing the physiological noise in the time-series (Ye et al., 2000) (although at the cost of BOLD sensitivity; Ghariq et al., 2014). In addition, performing ASL at ultra-high field (UHF; i.e., 7 T and higher) promises to be advantageous (Gardener et al., 2009; Ivanov et al., in press). The image SNR increases with field strength (Norris, 2003; Pohmann et al., 2016), which, for instance, improves white matter perfusion measurements with ASL (Gardener and Jezzard, 2015). In addition, the increased longitudinal relaxation times at higher fields (Rooney et al., 2007; Wright et al., 2008) reduce the label decay during the PLD and image acquisition leading to higher perfusion SNR. These advantages allow acquiring larger brain coverage and/or using longer PLD to avoid vascular artefacts, which are due to incomplete transfer of the labeled blood from the arterial tree to the local tissue. The advantages of UHF for BOLD imaging, demonstrated in numerous studies (e.g. Uludag et al., 2009; van der Zwaag et al., 2009; Donahue et al., 2011), and references therein), render simultaneous CBF and BOLD imaging using ASL at 7 T particularly attractive.

Despite the aforementioned gains, UHF ASL has not found widespread use in humans due to significant technical challenges. First, the spatial homogeneity and efficiency of the labeling are significantly degraded at UHF due to B_0- and B_1^+-inhomogeneities (Teeuwisse et al., 2010; Luh et al., 2013). Second, SAR constraints at 7 T make not only spin-echo-based (SE) approaches impractical, but also constrain the utilization of some widely-used 3 T ASL techniques at 7 T, such as pCASL labeling and background suppression. As a consequence, to remain within SAR limits, many UHF ASL implementations employ poor temporal resolutions that are not compatible with the requirements of adequately sampling the fMRI hemodynamic response (Ghariq et al., 2012; Luh et al., 2013; Zuo et al., 2013; Bause et al., 2016; Zimmer et al., 2016). For example, the increased power deposition at 7 T leads to doubling of the minimum achievable repetition time (TR) of pCASL at 3 T, even with low flip-angle readouts (Zuo et al., 2013; Wang et al., 2015b). Third, resolution loss along the phase-encoding direction and blurring in echo-planar imaging (EPI) can be observed for readout lengths typically used at lower fields due to the faster T_2^* decay at UHF (Farzaneh et al., 1990; de Zwart et al., 2006).

Parallel imaging addresses some of these issues by shortening the EPI readout and reducing the effective echo spacing. Thus, using parallel imaging reduces the image blur and geometric distortions due to off-resonance effects (de Zwart et al., 2006), while it facilitates increased temporal resolution or brain coverage, reducing the minimum echo time (TE) possible and/or enabling multiple echoes. Acquisition at shorter TE increases the perfusion-weighted signal (St Lawrence and Wang, 2005), while multi-echo approaches can better characterize the CBF and BOLD time-courses obtained from the ASL data. Since parallel imaging involves data undersampling, it also leads to decreases in image SNR and to a smaller extent temporal SNR (tSNR) (de Zwart et al., 2006).

The improved image SNR at 7 T compared to 1.5 and 3 T can also be utilized to image the human brain at higher spatial resolution. Pfeuffer and colleagues demonstrated at 7 T in humans that functional CBF mapping has superior spatial specificity than the typically-employed gradient-echo (GE) BOLD signal (Pfeuffer et al., 2002). Decreases in the voxel volume lead to proportional reduction in the ASL SNR, which render high-resolution perfusion imaging particularly challenging. In practice, to obtain sufficient SNR in ASL at 3 T, low spatial resolutions (above 3 mm isotropic) are utilized. Therefore, only a few studies have shown CBF maps with in-plane resolution below 1.5 mm (Duong et al., 2002; Pfeuffer et al., 2002; Zuo et al., 2013). It is worth noting that these studies utilized diverse acquisition approaches – SE, GE and turbo-FLASH (TFL), but were all performed at 7 T, indicating its potential for high-resolution CBF imaging.

In this work, we explore the benefits offered by a custom 7 T FAIR QUIPSS II (Wong et al., 1998) variant with optimized labeling RF pulses and dielectric pads (Ivanov et al., in press), in comparison to conventional 3 T ASL techniques for concurrent (functional) CBF and BOLD imaging. To facilitate a direct across-field comparison, FAIR QUIPSS II was also utilized at 3 T. Moreover, other commonly employed ASL techniques, such as PICORE Q2TIPS (Luh et al., 1999) and pCASL, were also acquired at 3 T. Furthermore, 2D EPI readouts and partial brain coverage were selected for their widespread availability and temporal efficiency allowing optimal conditions for concurrent functional CBF and BOLD experiments. In a second set of experiments, we additionally investigated the influence of spatial resolution within the aforementioned constraints in a subset of the techniques – pCASL and FAIR at 3 T along with the optimized 7 T FAIR. The in-plane resolution was varied between 3.0 mm (conventional) and 1.5 mm (high), while dual-echo data was enabled using the GRAPPA (Griswold et al., 2002) parallel imaging approach. In summary, we systematically examined the influence of imaging parameters affecting the ASL signal quality, including field strength, labeling scheme, spatial resolution, echo time, and use of parallel imaging, to determine their utility for achieving high-quality, high-spatial resolution functional CBF and BOLD imaging.

Materials and methods

Subjects

Nine healthy volunteers (4 females, age range 24–42 years) took part in Experiment 1 investigating the effects of ASL sequence choices on perfusion sensitivity, control sensitivity and absolute CBF values. Eight healthy volunteers (4 females, age range 24–30 years) took part in Experiment 2 investigating the effects of spatial resolution and echo time on perfusion sensitivity, control sensitivity as well as on CBF and BOLD functional sensitivity. All participants had normal or corrected-to-normal vision. Written informed consent was obtained from all participants according to the approval of the study protocol by the Ethical Committee of the Faculty of Psychology and Neuroscience, Maastricht University.

Data acquisition

Measurements were performed on a 3 T MAGNETOM Prisma Fit

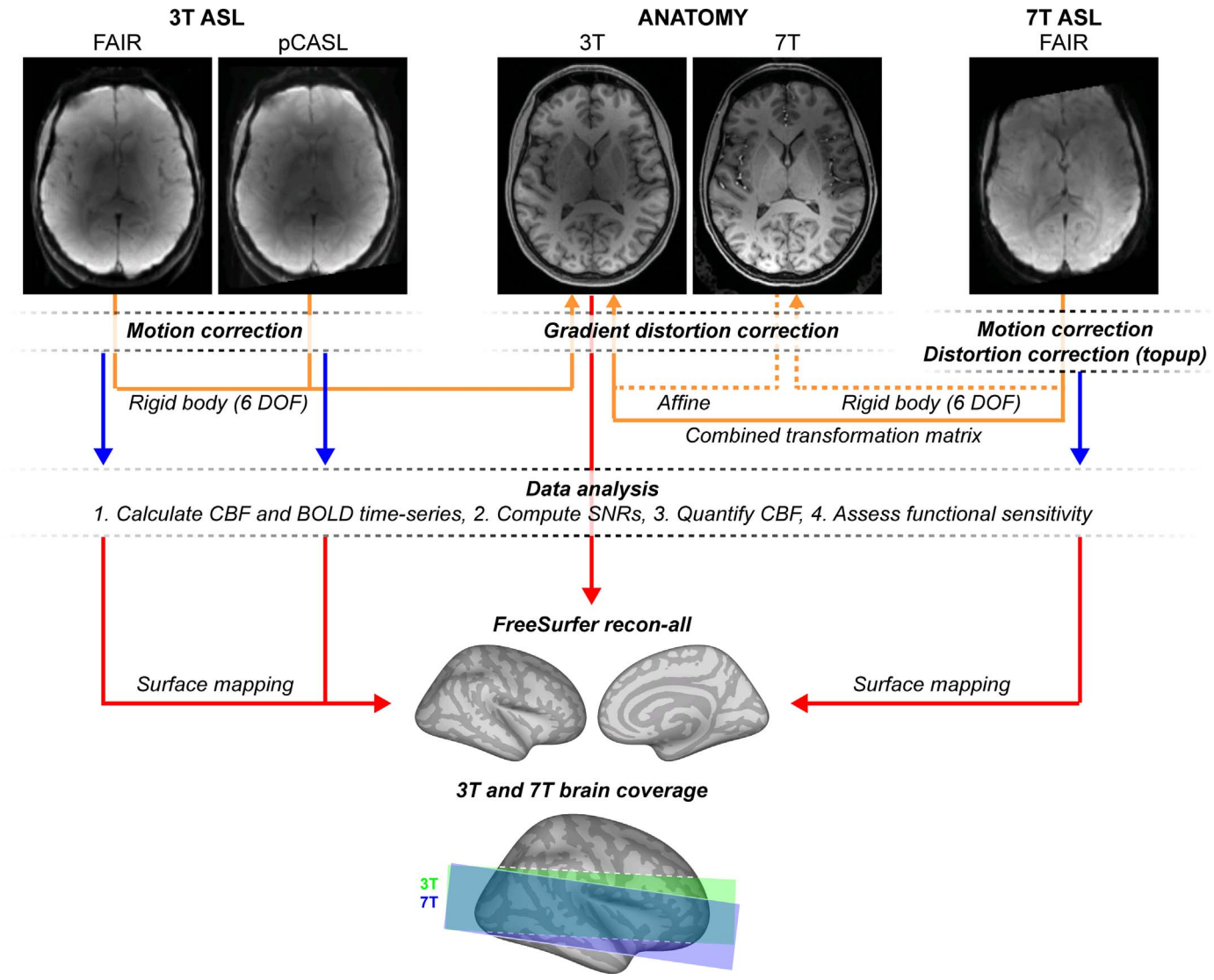

Fig. 1. Analysis pipeline.

and a 7 T whole-body research scanner (Siemens Healthcare, Erlangen, Germany) using a 64-channel head/neck coil (Siemens Healthcare, Erlangen, Germany) and 32-channel head coil (Nova Medical, Wilmington, MA, USA), respectively. In order to improve the labeling efficiency at 7 T, two rectangular 18×18 cm^2 dielectric pads with 5 mm thickness (Teeuwisse et al., 2012) were placed on either side of the head at the level of the temporal lobes. At both 3 T and 7 T, the eye centers were taken as a reference for the magnet isocenter position (~ level of pons), instead of the typically chosen eyebrows (~level of basal ganglia) to minimize B_0 offsets in the labeling region. Furthermore, the brain-feeding arteries were aligned with the B_0 field by adding cushions below the necks of the participants when necessary. These measures were previously shown to improve labeling efficiency at 7 T (Ivanov et al., in press). Half of the participants were first scanned at the 3 T scanner and then immediately transferred to the 7 T scanner, and vice versa for the other half of the participants. The two scanners are located within the same building at a walking distance of a few meters.

ASL sequences

All experiments used prototype ASL sequences written in-house. Fig. 1 schematically shows the analysis pipeline used in this study. In Experiment 1, three ASL schemes, namely FAIR QUIPSS II (Wong et al., 1998), PICORE Q2TIPS (Luh et al., 1999) and pCASL (Wu et al., 2007; Dai et al., 2008), were acquired at the 3 T and one ASL scheme, namely FAIR QUIPSS II, at the 7 T. All sequences employed a 2D EPI readout. The labeling at the 7 T was achieved using a tr-FOCI inversion pulse (Hurley et al., 2010), while at 3 T a C-FOCI inversion pulse was used. The remaining saturation pulses applied (in PASL and pCASL) were implemented as in the respective vendor's implementations. For the rest of the paper, we will refer to them with the following abbreviations: *3 T FAIR*, *3 T PQ2T*, *3 T pCASL* and *7 T FAIR*, respectively. Thirteen slices were acquired with a voxel resolution of 3.0 mm isotropic and angulated in order to cover the visual and auditory cortices. For all schemes, one baseline perfusion run was acquired with 96 time points duration (i.e. 4 min). Further, an additional 3 T pCASL run was obtained with identical readout, but labeling duration (τ) and PLD of 1500 and 1580 ms, respectively, close to the ASL white paper recommendations accounting for the distribution of arterial arrival times across the brain (Alsop et al., 2015). The duration of this run (which in the following will be identified with the abbreviation *WHITEP*) was matched to that of the others, but the TR was 3.6 s, hence resulting in 66 time points. The position of the pCASL labeling plane was 60 mm inferior to the slice stack, usually directly below the cerebellum. The inversion slab thickness for the 3 T FAIR, 3 T PQ2T and 7 T FAIR was 60 mm and the QUIPSS II/Q2TIPS saturation slabs of 100 mm thickness were applied 20 mm inferior to the lowest slice acquired. The order of acquisitions at the 3 T was

Table 1
ASL sequence parameters of Experiment 1. All sequences employed a 2D EPI readout. In the central column, all parameter values are reported, while in the left and right column values are displayed only when different among the sequences. The symbol '—' indicates that the corresponding parameter does not apply for that sequence.

	3 T FAIR, PQ2T, pCASL	WHITEP	7 T FAIR
In-plane resolution [mm]		**3.0**	
Slice thickness [mm]		3.0	
TR [ms]	2500	3600	2500
TI1/TI2 [ms] or	700/1800 (FAIR, PQ2T)	—	700/1800
τ/PLD [ms]	975/1005 (pCASL)	1500/1580	—
Number of slices		13	
TE [ms]		13	
Base resolution		64	
Echo spacing [ms]	0.51	0.51	0.53
Partial Fourier		6/8	
GRAPPA		off	
Slice time acquisition [ms]	30.4	30.4	31.6
Readout duration [ms]	24.48	24.48	25.44

pseudo-randomized across the participants. The acquisition parameters were matched as closely as possible across ASL schemes and field strengths (see Table 1 for sequence parameters details). At 7 T, one M_0 image was acquired using the same sequence but with no magnetization preparation and TR increased to 20 s. At 3 T, a separate M_0 acquisition was not necessary since the M_0 acquisition is implemented in the sequence acquisition itself as the 1st volume of the run (but only if no parallel imaging is used). At each scanner, one high-resolution anatomical scan was acquired: MPRAGE sequence at 3 T with 1.0 mm isotropic resolution (TE/TI/TR =2.18/1040/2400 ms and 8 degrees flip angle); MP2RAGE sequence at 7 T with 0.9 mm isotropic resolution (TE/TI1/TI2/TR =2.39/900/2750/4500 ms and flip angle 1/2=5/3°).

In Experiment 2, two ASL schemes were used at the 3 T, namely FAIR QUIPSS II and pCASL, and one ASL scheme at the 7 T, namely FAIR QUIPSS II. GRAPPA factor 3 (using the FLEET approach for reference lines acquisition (Polimeni et al., 2016)) was employed for all variants, in order to allow the acquisition of the highest in-plane resolution and the 2nd echo (TEs =13 and 37 ms) within the fixed TR of 2.5 s. All imaging parameters were matched as closely as possible across ASL schemes and field strengths (see Table 2 for details).

For each combination of ASL variant and in-plane resolution in Experiment 2, one functional run of 204 time points (i.e. 8.5 min) was acquired while participants attended to the visual stimulation. The stimulation protocol of each run consisted of an initial rest period (gray screen) of 30 s and 8 blocks each consisting of 25 s 8 Hz flickering-checkboard hemifield stimulation followed by 35 s rest. A white cross, always present in the center of the screen, was used as fixation point. In order to stimulate the same portion of the visual field at the 3 T and 7 T scanner, the size of the projected visual stimulus was adjusted according to the scanner specific stimulus setup to yield 6.5 degrees visual angle stimulation at both scanners. In order to avoid order effects, the acquisition order of the different resolutions was pseudo-randomized across participants as well as that of the ASL schemes at the 3 T. For each ASL implementation in Experiment 2, one M_0 image was acquired with a TR increased to 20 s and no magnetization preparation. 7 T ASL runs were followed by the acquisition of 3 volumes (=7.5 s) with the same sequence but with opposite phase-encoding direction to allow for offline distortion correction with the reversed-gradient approach. High-resolution (0.7 mm isotropic) anatomical scans were acquired at each scanner. An MPRAGE sequence (TE/TI/TR =2.11/1040/2400 ms and 8 degree flip angle at 3 T and TE/TI/TR =2.47/1500/3100 ms and 5 degree flip angle) was followed by a proton-density-weighted scan with identical imaging parameters apart from the lack of inversion pulse and shorter TR (1890 ms at 3 T and 1660 ms at 7 T). This was done to allow correction for receive bias fields in a consistent manner across both scanners (Van de Moortele et al., 2009).

Preprocessing

Motion correction was performed using SPM8 (http://www.fil.ion.ucl.ac.uk/spm/software/spm8/). In order to treat all ASL runs equally, each ASL run (and the corresponding M_0 image) was realigned independently from the other runs, by realigning all volumes and the M_0 image to the first volume of that run. Also 1st and 2nd echo images of Experiment 2 were treated separately for motion correction as well as for the rest of preprocessing described below. After realignment, 7 T ASL runs were distortion corrected using the reversed-gradient approach *(TOPUP)* as implemented in FSL (http://fsl.fmrib.ox.ac.uk/fsl) (Andersson et al., 2003; Smith et al., 2004). No spatial smoothing was applied to preserve the spatial fidelity of the data. The temporal mean of each ASL run was computed and used to calculate the coregistration matrix with the anatomical scan of the corresponding scanning session. Rigid-body coregistration (i.e., using 6 parameters: 3 translation and 3 rotation parameters) between each ASL run and anatomical scan was performed using FLIRT (Jenkinson et al., 2002). In order to align the data from the two different scanners, an affine transformation between 7 T and 3 T anatomical scan was calculated using RobustRegister (mri_robust_register; Reuter et al., 2010). Finally, a mask representing the overlap volume between all ASL slabs (both 3 T and 7 T sessions, all ASL schemes, and all resolutions

Table 2
ASL sequence parameters of Experiment 2. In the central column, all parameter values are reported, while in the left and right column values are displayed only when different among the sequences. Values identical across in-plane resolutions are reported only once.

	3 T FAIR				3 T pCASL				7 T FAIR			
In-plane resolution [mm]	**1.5**	**2.0**	**2.5**	**3.0**	**1.5**	**2.0**	**2.5**	**3.0**	**1.5**	**2.0**	**2.5**	**3.0**
Slice thickness [mm]						3.0						
TR [ms]						2500						
TI1 or τ [ms]			700			925				700		
TI2 or PLD [ms]			1800			875				1800		
Number of slices			10			10				12		
TE1 [ms]						13						
TE2 [ms]						37						
Delay after 1st echo [ms]	0	6	7	8	0	6	7	8	0	6	7	8
Base resolution	128	96	78	64	128	96	78	64	128	96	78	64
Echo spacing [ms]	0.69	0.68	0.68	0.68	0.69	0.68	0.68	0.68	0.69	0.68	0.68	0.69
Partial Fourier	6/8	6/8	7/8	off	6/8	6/8	7/8	off	6/8	6/8	7/8	off
GRAPPA					3							
Slice time acquisition [ms]	56.8	49.6	47.8	46.0	56.8	49.6	47.8	46.0	54.8	50.5	48.8	47.3
Readout duration [ms]	22.1	16.3	15.6	15.0	22.1	16.3	15.6	15.0	22.1	16.3	15.6	15.2

for Experiment 2) was computed. The anatomical images from both the 3 T and 7 T sessions were corrected for gradient non-linearities using the vendor-provided software routines, and affine registration was applied to achieve adequate coregistration between them.

The only exceptions to this pipeline were made for subject 1, 2, and 8 of Experiment 1: For subject 1 and 2, no opposite phase-encoding images were acquired for the 7 T ASL run, thus no distortion correction was performed. For subject 8, no 3 T anatomy was available due to time constraints during the scanning session. Therefore, ASL data from the 3 T session were manually registered to the 7 T anatomical scan.

In both Experiment 1 and 2, automatic segmentation of the subject's anatomy was performed on the 3 T anatomical scan (except subject 8) using FreeSurfer (https://surfer.nmr.mgh.harvard.edu/) and the recon-all pipeline. The segmentation obtained was visually inspected and no manual corrections were needed for any subject.

Perfusion calculation

Each motion-corrected (and distortion-corrected, in case of 7 T) ASL run was separated into control and label time-series. For Experiment 2, only the 1st echo signal was considered. If not further specified, analyses and results concerning Experiment 2 will refer to the 1st echo images for the rest of the paper. Subtraction of the label from the control images yielded a perfusion-weighted time-series and its temporal mean a perfusion-weighted map.

Quantification of the perfusion map was performed according to the model described in Alsop et al. (2015). TI_2 and PLD values were calculated for each slice, as slices were acquired using a 2D EPI readout with an ascending slice order. The parameters used were: 1.650 s for the longitudinal relaxation time of blood at 3 T (Lu et al., 2004; Zhang et al., 2013) and 2.100 s at 7 T (Dobre et al., 2007; Gardener et al., 2009; Zhang et al., 2013); 0.9 ml/g for the brain/blood partition coefficient; and for the labeling efficiency 0.98 in 3 T FAIR and 3 T PQ2T, 0.95 for 7 T FAIR, and 0.85 for 3 T pCASL and WHITEP.

A mean GM perfusion value was calculated considering all voxels included in an anatomically defined GM mask derived from the anatomical segmentation. Differences in mean GM perfusion values for the different ASL implementations were tested using a one-way repeated measures ANOVA for Experiment 1 and two-way repeated measures ANOVA for Experiment 2. In the first case, ASL scheme (i.e. 3 T FAIR, 3 T PQ2T, 3 T pCASL, WHITEP or 7 T FAIR) was the only independent variable, in the latter also voxel volume (e.g. 1.5×1.5×3.0 mm^3, 2.0×2.0×3.0 mm^3, ...) was taken into account as a second independent variable. Repeated measures ANOVA, here and for the rest of the paper, were computed in SPSS using the Greenhouse-Geisser correction (which accounts for unequal variances of the differences between all factor combinations). P-values of pairwise comparisons are reported according to Fisher's Least Significance Differences (LSD, unadjusted probabilities).

Finally, the influence of using parallel imaging (GRAPPA 3) on the baseline perfusion values was tested using the data from Experiment 1 and 2 for the common voxel resolution of 3.0 mm isotropic and the common ASL schemes (3 T FAIR, 3 T pCASL, and 7 T FAIR). A two-way repeated measure ANOVA was computed using ASL scheme as a within-subject factor and parallel imaging as a between-subject factor.

SNR and CNR measures

The signal quality of the different ASL acquisitions was compared by assessing the perfusion tSNR, control tSNR, perfusion CNR, and control CNR. The duration of the additional acquisitions used to distortion-correct the 7 T ASL images was not considered in the SNR/CNR evaluations.

Voxel-wise perfusion tSNR was calculated by dividing the mean of the perfusion time-series in each voxel by its standard deviation. With the term *control tSNR* we indicate the tSNR of the control time-series, which approximates the tSNR usually measured in standard BOLD fMRI. Control tSNR was computed voxel-wise by dividing the temporal mean of the control time-series by its standard deviation. This quantity was calculated after filtering the control time-series with a nonlinear high-pass filter of 60 s using the -bptf option of fslmaths (from the FSL toolbox http://fsl.fmrib.ox.ac.uk/fsl).

The perfusion and control CNR were calculated from the perfusion and control time-series, respectively, dividing the standard deviation of the activation signal by the standard deviation of the noise (Welvaert and Rosseel, 2013; cfr. Definition 4). For this calculation, only voxels identified as active (see following section “CBF and BOLD activation”) were considered. The same amount of volume across different sequences, resolutions, and contrasts was used in order to guarantee a fair statistical comparison. For Experiment 2, all four quantities were calculated also for the 2nd echo time-series.

Differences in perfusion and control tSNR, and CNR for the different ASL implementations were tested using a one-way repeated measures ANOVA with ASL scheme as factor for Experiment 1 and two-way repeated measures ANOVA with ASL scheme and voxel volume as factors for Experiment 2.

The decreases in the perfusion or control tSNR due to a certain factor, such as use of parallel imaging acceleration, TE or change in voxel volume with respect to a given other reference setting, were obtained using the equation:

$$Loss = \frac{tSNR_{Ref} - tSNR_x}{tSNR_{Ref}} \quad (1)$$

CBF and BOLD activation

In Experiment 2, the functional sensitivities of the CBF and BOLD signal were evaluated by comparing the significant activation detected using the full GLM ASL model (Mumford et al., 2006; Hernandez-Garcia et al., 2010). In this framework, the raw ASL signal is modeled by four predictors:

$$y(t) = \beta_0 + \beta_1 x_1(t) + \beta_2 x_2(t) + \beta_3 x_3(t) + \epsilon(t) \quad (2)$$

where $y(t)$ is the signal intensity of a particular voxel at the time point $t = 1,\ldots,n$, the first regressor $x_0(t) = 1$ and its coefficient parameter β_0 represent the baseline MR signal. The second regressor $x_1(t)$ consists of an alternation of +0.5 and −0.5 describing the ASL zig-zag signal that represents the acquisition of control and label pairs. Thus, its coefficient parameter β_1 represents the relative baseline perfusion. The third regressor $x_2(t)$ and its coefficient β_2 describe the relative CBF signal change due to activation, while the fourth regressor $x_3(t)$ and its coefficient β_3 the BOLD signal change. Finally, $\epsilon(t)$ is the error term. The activation BOLD predictor x_3 is built convolving a box car function representing the stimulus block with a gamma function in order to account for the hemodynamic response delay. The activation CBF predictor x_2 is obtained by multiplying the activation BOLD predictor x_3 with the baseline CBF predictor x_1.

GLM analysis was performed using FEAT v6.00 (from the FSL toolbox http://fsl.fmrib.ox.ac.uk/fsl) including a pre-processing step of high-pass filtering (60.0 s cutoff) and FILM prewhitening. Statistical results were corrected for multiple comparisons using a cluster-size approach: voxel Z-statistics was thresholded using a Z-threshold of 2.3, then the resulting clusters were thresholded using a cluster p-value threshold of 0.05. Subject 6 was excluded from this analysis as no activation was detected for multiple acquisitions due to excessive motion. For all other subjects, activation maps were masked projecting back into the functional space using the binary mask representing the intersection of all ASL slabs acquired for that subject. In this manner, we excluded that differences in the amount of activation detected were caused by different coverage of the ASL slabs. Thanks to careful positioning of the slices, the intersection across

all ASL runs resulted in a consistent portion of the acquired ASL slabs for all subjects (see Fig. 1 for an illustration). Differences in the amount of activated volume detected by the activation CBF and BOLD predictors for the different ASL implementations were tested using a three-way repeated measures ANOVA with signal (CBF or BOLD signal), ASL scheme (3 T FAIR, 3 T pCASL, or 7 T FAIR), and voxel size (corresponding to 1.5, 2.0, 2.5, and 3.0 mm in-plane resolution) as factors. Each subject's activation maps were projected on the cortical surface and averaged for display purposes only.

The full GLM ASL analysis and subsequent statistical evaluation were repeated for the 2nd echo signal of Experiment 2.

Perfusion territories

To assess differences in the CBF distribution across the cortex due to the different labeling schemes, we defined perfusion territory masks corresponding to the anterior, middle and posterior cerebral arteries (ACA, MCA, and PCA, respectively). The territory definition was based on the atlas provided by (Tatu et al., 2012). To build the territory masks in a semi-automatic way, the FreeSurfer automatic segmentation following the Desikan-Killiany' cortical atlas (Desikan et al., 2006) was used, with the exception of the distinction between occipital and parietal superior gyrus for which the Destrieux' cortical atlas (Destrieux et al., 2010) was utilized. The segmented GM areas were re-labeled as ACA, MCA or PCA according to the Tatu's atlas. Additionally, a left and right distinction was made yielding 6 perfusion territory masks for each subject (see Table ST2 in Supplementary Material for a detailed list of the included areas and Fig. 7 for an example of the resulting masks). Differences in CBF across perfusion territories were statistically assessed using four-way repeated measures ANOVA with ASL scheme, voxel volume, perfusion territory and laterality as factors for Experiment 2, and three-way repeated measures ANOVA with ASL scheme, perfusion territory and laterality as factors for Experiment 1.

Results

Perfusion maps

Fig. 2A shows an axial slice of the quantitative perfusion maps obtained for a representative subject from each ASL acquisition in Experiment 1. Overall, the perfusion maps look similar, however they present some local differences. A clear contrast between GM and WM regions is visible in all maps, but the GM's perfusion signal is generally lower in the 7 T FAIR map. The sagittal sinus appears bright for the 3 T FAIR scheme, which is a well-known artifact of the labeling geometry causing tagged venous blood to inflow from superior slices (Wong et al., 1997; Cavusoglu et al., 2009). The sparser perfusion map appearance in the posterior part of the brain and the higher values in several isolated voxels in the 3 T pCASL are the result of the short PLD used.

Fig. 2B shows the mean GM CBF averaged across subjects (single-subject and group values are reported in Supplementary Table ST1). Note that the values indicated by circles in the gray box represent the acquisitions with no parallel imaging utilized. 7 T FAIR yields always the lowest GM CBF values, whereas 3 T PASL and pCASL yield very similar GM CBF values for the 3.0 mm isotropic measurements without parallel imaging (Experiment 1: '7 T FAIR vs. 3 T FAIR' $p < 0.001$, '7 T FAIR vs. 3 T PQ2T' $p < 0.001$, '7 T FAIR vs. 3 T pCASL' $p=0.001$, '7 T FAIR vs. WHITEP' $p=0.018$). 3 T FAIR delivers the highest GM CBF values for the acquisitions using parallel imaging (GRAPPA 3, Experiment 2: '3 T FAIR vs. 3 T pCASL' $p \leq 0.006$, '3 T FAIR vs. 7 T FAIR' $p < 0.001$, '3 T pCASL vs. 7 T FAIR' $p=0.001$). For Experiment 2, the mean GM CBF was generally not influenced by the voxel size: a significantly different mean GM CBF value was found only for the 1.5 mm versus the 2.0 mm and 2.5 mm in-plane resolution ($p < 0.001$ for both comparisons).

Finally, considering the acquisitions with ASL scheme and voxel size common between Experiment 1 and 2 (i.e. the 3 T FAIR, 3 T pCASL, and the 7 T FAIR, all at the 3.0 mm isotropic voxel size), we compared the GM CBF values obtained with or without parallel imaging (i.e. Experiment 2 using GRAPPA 3 vs. Experiment 1 without GRAPPA). A significant effect was found for the ASL scheme factor ($p < 0.001$), but not for the parallel imaging factor and the interaction term 'ASL scheme * Parallel imaging' ($p=0.945$ and $p=0.174$, respectively).

SNR measures

Temporal SNR

Fig. 3 shows an example of the perfusion tSNR maps obtained in Experiments 1 and 2. Mean perfusion tSNRs as functions of the voxel

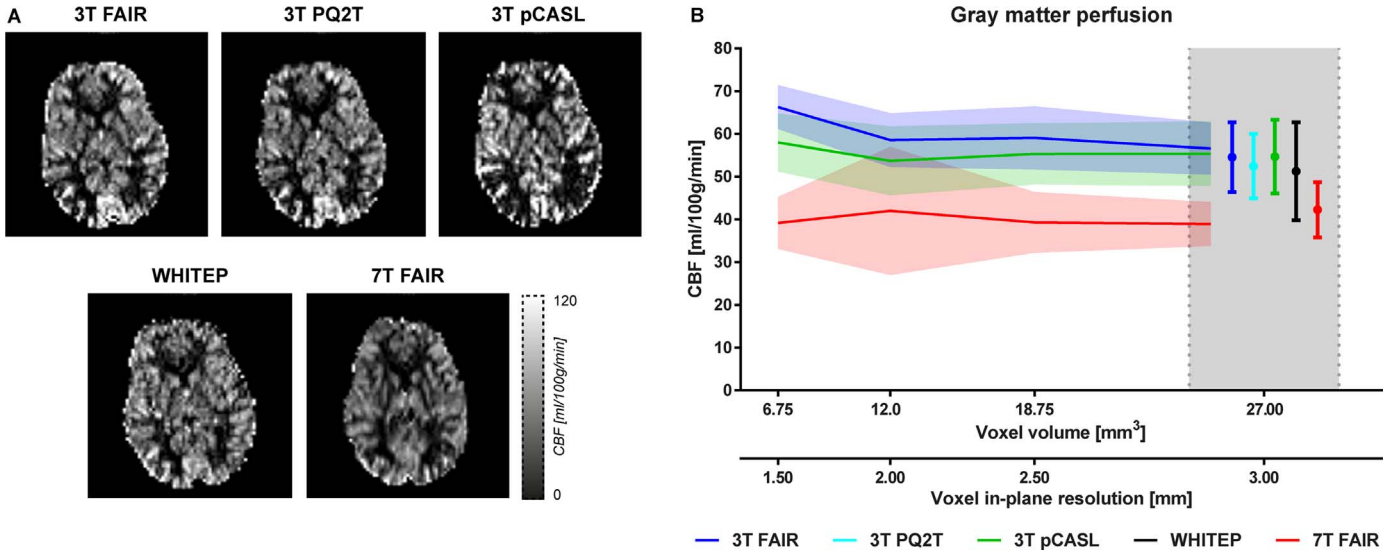

Fig. 2. Quantitative perfusion maps and mean GM CBF values. A) One slice of the perfusion maps obtained with each ASL scheme for a representative subject from Experiment 1; B) Mean GM perfusion values plotted as a function of the voxel volume. Shades and error bars represent the standard deviation across the subjects. Two x-axes are shown for clarity in (B): the first x-axis represents the voxel volume corresponding to each in-plane resolution (indicated in the second x-axis) and a slice thickness of 3.0 mm. Points connected by continuous lines represent the results from Experiment 2, in which the voxel volume varied between $1.5\times1.5\times3.0$ mm^3 and $3.0\times3.0\times3.0$ mm^3. Results from Experiment 1 with voxel size $3.0\times3.0\times3.0$ mm^3 are indicated by a circle within the gray box and are slightly shifted apart from each other and from the last point of Experiment 2 for visualization purposes.

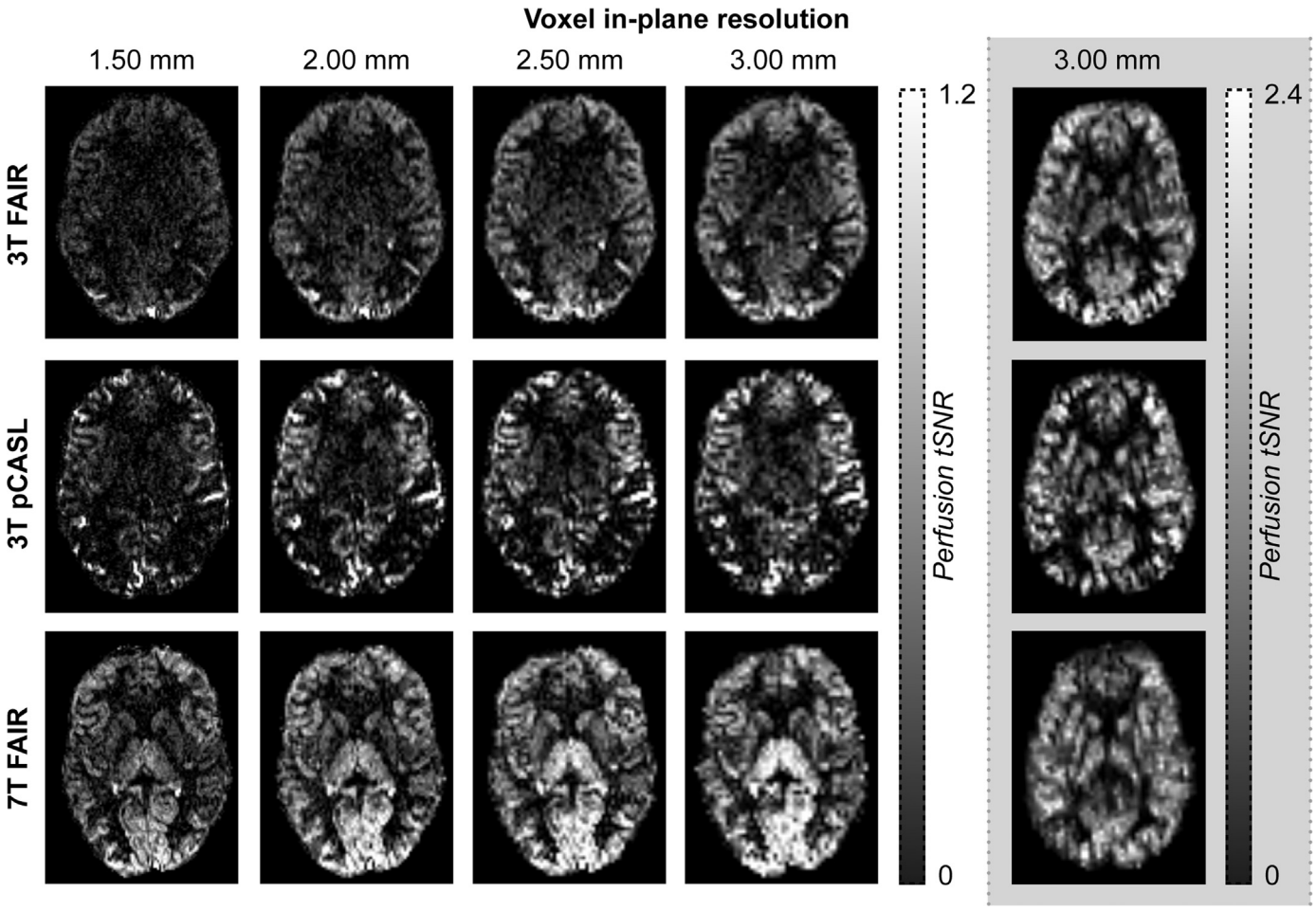

Fig. 3. Perfusion tSNR maps. The perfusion tSNR maps of two representative subjects are shown for the two experiments (Experiment 2 on the left and Experiment 1 on the right with the gray background).

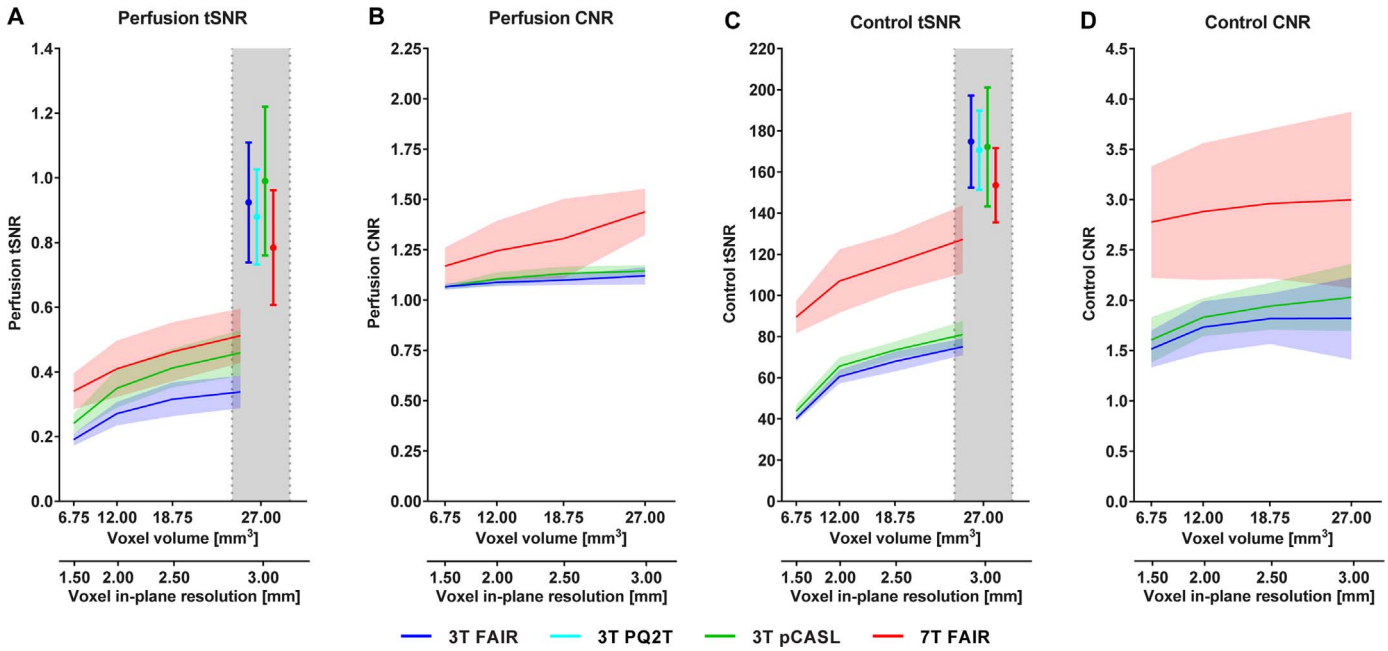

Fig. 4. TSNR and CNR measures in the anatomical GM masks. Panel A, B, C, and D show perfusion tSNR, perfusion CNR, control tSNR and control CNR, respectively, as a function of voxel volume. Continuous lines and circle symbols indicate measures corresponding to TE =13 ms for Experiment 2 and 1, respectively. Shades and error bars represent standard deviations across the subjects.

size and the use (or not) of parallel imaging are shown in Fig. 4A (continuous lines and circle symbols). As expected, perfusion tSNR increases with voxel volume and has higher values for acquisitions without parallel imaging. No significant differences in perfusion tSNR between the 3 T acquisitions were observed for Experiment 1. Further, in Experiment 1 7 T FAIR has significantly lower perfusion tSNR than 3 T FAIR and 3 T PQ2T ($p=0.021$) as well as 3 T pCASL ($p=0.028$). In contrast, 7 T ASL yields higher perfusion tSNR values than 3 T at all voxel sizes when parallel imaging is used ($p < 0.038$ for all comparisons except for $p=0.124$ for '7 T FAIR vs. 3 T pCASL' at 2.5 mm; Experiment 2). Within the 3 T ASL sequences, pCASL has higher perfusion tSNR than FAIR ($p < 0.001$ for all resolutions). The loss in perfusion tSNR due to the use of GRAPPA factor 3 was largest for 3 T FAIR (63%), followed by 54% for 3 T pCASL and only 35% for 7 T FAIR, indicating reduced thermal noise (i.e. increased image SNR) at 7 T. Using the 3.0 mm isotropic resolution from Experiment 2 as a reference, the perfusion tSNR decreased very similarly for 3 T FAIR, 3 T pCASL and 7 T FAIR when increasing the in-plane resolution to 2.5 and 2.0 mm. The differences between 7 T and 3 T perfusion tSNR loss become large for the 1.5 mm resolution: 46% for 3 T vs. 33% for 7 T. Note that the 7 T/3 T tSNR ratio, and hence the benefit of 7 T, is largest for the highest spatial resolution.

Fig. 4C shows the tSNR values obtained from the high-pass-filtered control time-series. A consistent trend between different ASL implementations (ASL schemes, voxel volumes, and use or not of parallel imaging) was observed: 7 T ASL had higher control tSNR than 3 T ASL when parallel imaging was employed ($p < 0.001$ for '7 T FAIR vs. 3 T FAIR' and '7 T FAIR vs. 3 T pCASL'), and lower control tSNR than 3 T ASL for implementations without parallel imaging ($p=0.017$ for '3 T FAIR vs. 7 T FAIR', $p=0.025$ '3 T PQ2T vs. 7 T FAIR', and $p=0.056$ for '3 T pCASL vs. 7 T FAIR'). The control tSNR loss due to the GRAPPA factor 3 used was slightly larger for the 3 T FAIR than for 3 T pCASL – 57% vs. 53%. In comparison, the control tSNR loss due to use of the same acceleration factor for 7 T FAIR was only 17%, further supporting the claim of higher SNR at 7 T. In Experiment 2, the control tSNR increased significantly with increasing voxel volume ($p < 0.001$ for all comparisons). Taking the 3.0 mm isotropic resolution from Experiment 2 as a reference, the control tSNR decreased by a similar amount for all approaches when increasing the in-plane resolution to 2.5 and 2.0 mm. The differences between 7 T and 3 T control tSNR loss are again largest for the 1.5 mm resolution – 30% for 7 T FAIR and 46% for both 3 T ASL schemes.

CNR

The main findings for the CNR are similar to those for the tSNR. Fig. 4B illustrates the perfusion CNR increasing as a function of the voxel volume for all ASL implementations. 7 T FAIR delivered the highest perfusion CNR ($p < 0.040$ for all comparisons), while 3 T pCASL showed a tendency to higher values with respect to 3 T FAIR (with a significance of $p=0.025$ only for the 2.5 mm case). The control CNR values, shown in Fig. 4D, were characterized by a significant main effect of both voxel volume and ASL scheme factors ($p=0.001$ for both effects and no significant interaction). 7 T FAIR delivered significantly higher control CNR values than 3 T FAIR ($p=0.001$) and 3 T pCASL ($p=0.002$), and 3 T pCASL significantly higher than 3 T FAIR ($p=0.031$).

TSNR and CNR were computed also using the 2nd echo (i.e. TE=37 ms) acquired in Experiment 2. Supplementary Fig. S1 in the Supplementary Material shows the expected decrease in perfusion tSNR, perfusion CNR and control tSNR and increase in control CNR at the longer TE.

CBF and BOLD activation

The full GLM ASL analysis showed significant activations for both CBF and BOLD signal (see Fig. 5). The activation clusters were mainly located in the right early visual cortex (EVC), as expected given the visual stimulation in the left visual field. Note that due to the interpolation when projecting the statistical maps on the cortical surface a lower statistical threshold was chosen for display purposes. The BOLD activation was more widespread and reached higher Z-statistics values in line with the higher tSNR observed for the BOLD signal with respect to CBF. In CBF activation, clusters outside EVC were detected only for the lowest resolution investigated (i.e. 3.0 mm isotropic) and 7 T FAIR. On the contrary, for BOLD activation, clusters outside EVC were detected for all voxel sizes and more strongly for 7 T FAIR. The general increase in the volume activated for increasing voxel sizes and the larger extent of activation detected for 7 T FAIR with respect to both 3 T acquisitions are evident from the plots in Fig. 6 (Panels A, and B referring to CBF and BOLD activation, respectively). The statistical tests resulted in $p < 0.001$ and $p=0.016$ for the interaction terms 'contrast * ASL scheme' and 'contrast * voxel volume', respectively. Further, the significant pairwise comparison for the simple two-way interactions were (for CBF/BOLD signal): $p=0.026$/$p=0.055$ for '2.0 mm vs. 1.5 mm', $p < 0.001$/$p=0.005$ for '2.5 mm vs. 1.5 mm', $p=0.023$/$p=0.012$ for '3.0 mm vs. 1.5 mm', $p=0.029$/n.s. for '3.0 mm vs. 2.0 mm'; n.s./$p=0.001$ for '7 T FAIR vs. 3 T FAIR', n.s./$p=0.001$ for '7 T FAIR vs. 3 T pCASL', n.s./$p=0.011$ for '3 T pCASL vs. 3 T FAIR', n.s. for all other pairwise comparisons. Finally, 3 T PCASL resulted in larger activated volume than 3 T FAIR for both CBF and BOLD signal (for CBF/BOLD signal: n.s./$p=0.011$).

Fig. 6C shows the volume significantly modulated according to the baseline CBF predictor. The increase in voxel volume resulted in an increase of the modulated volume with a significant effect observed for all comparisons ($p \leq 0.001$ for all comparisons). 7 T FAIR surpassed both 3 T ASL schemes ($p < 0.001$ for both comparisons), and 3 T pCASL was superior to 3 T FAIR ($p=0.002$).

The full GLM analysis was performed also for the 2nd echo data (see Supplementary Fig. S2) yielding results in agreement with the BOLD sensitivity depencence on GM T_2* at 3 T and 7 T.

Perfusion territories CBF

Fig. 7 shows the GM quantitative perfusion values averaged within each territory (which were defined in each individual's anatomical space) and then across the participants to obtain mean and standard error values for all ASL schemes of Experiment 1 and 2. The plots show that the pulsed ASL schemes (i.e. 3 T FAIR, 3 T PQ2T, and 7 T FAIR) result in a higher mean GM CBF in the PCA with respect to the ACA and MCA territory, while pCASL leads to a higher mean GM CBF in the MCA territory with respect to the other two, although for the WHITEP implementation the differences among territories are minimized. These different behaviors are reflected in the significance of the interaction 'ASL scheme * perfusion territory' ($p < 0.001$ for both Experiment 1 and 2).

Discussion

In this study, we compared an optimized 7 T PASL approach to several 3 T ASL techniques with respect to the quality and sensitivity of concurrently measured CBF and BOLD signals. To this aim, the same labeling scheme, namely FAIR QUIPSS II, was employed at both field strengths and a broad range of measurement parameters was considered: spatial resolution, parallel imaging and echo time. Furthermore, the influence of labeling scheme was also investigated by extending the comparison to alternative 3 T ASL techniques, such as PICORE Q2TIPS and pCASL. It is worth reiterating that the focus of this study has been on techniques that allow ASL acquisitions with a short TR (2.5 s) to ensure that a broad range of functional paradigms can be employed, which precluded the use of recent whole-brain SAR-intensive 7 T pCASL implementations (Ghariq et al., 2012; Luh et al., 2013; Wang et al., 2015a).

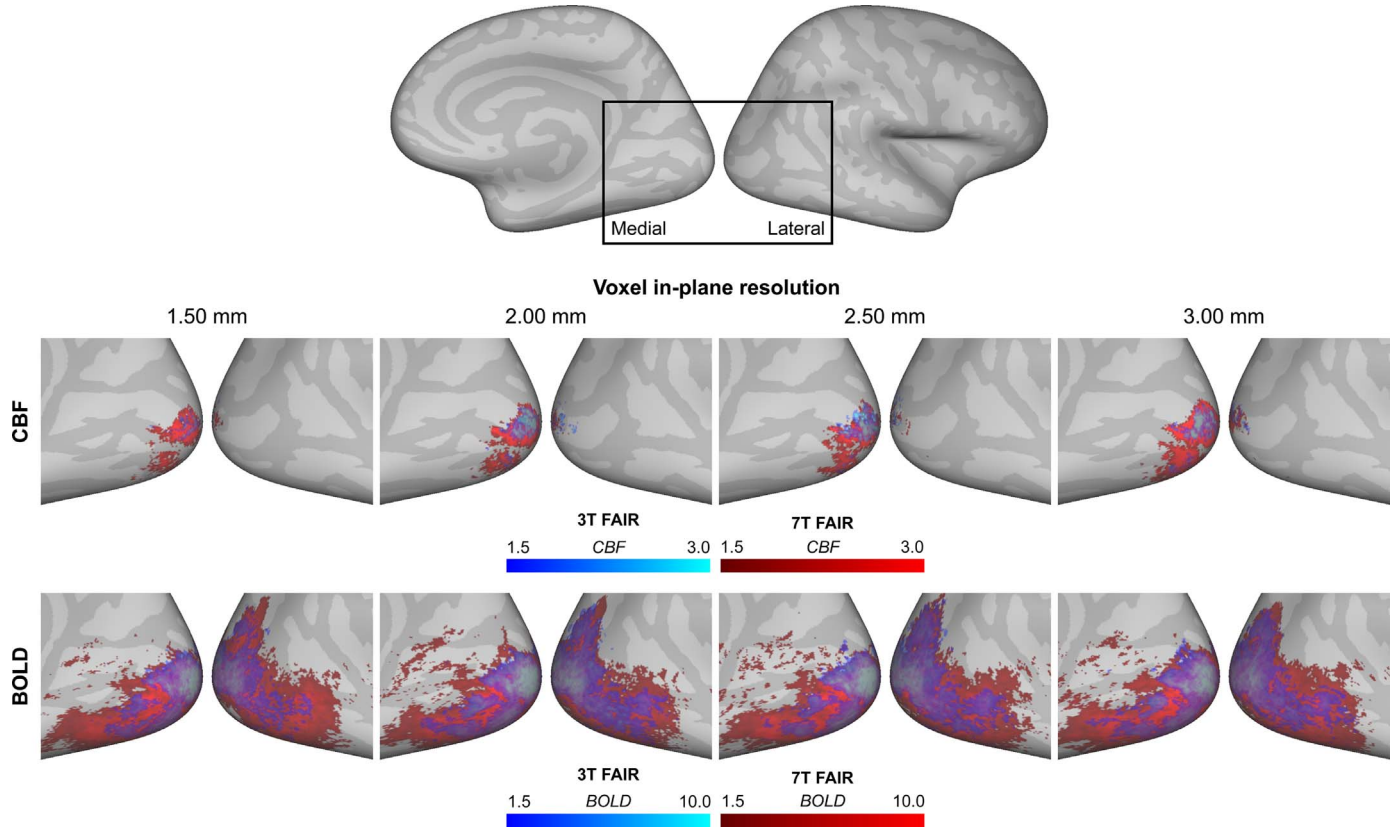

Fig. 5. CBF and BOLD activations. Significant activation detected by the CBF and BOLD predictors of the full GLM ASL model for the different in-plane resolutions: results from 3 T FAIR are overlaid on the 7 T FAIR ones to facilitate across-field-strength comparison. 3 T pCASL activation maps were very similar to those from 3 T FAIR and are therefore not shown. The top row shows the CBF activation and the bottom row the BOLD activation. The Z-values are color-coded from dark to light blue for 3 T FAIR and from dark to light red for 7 T FAIR. A different maximum value was chosen for CBF and BOLD (i.e. 3.0 and 10.0, respectively) to better suit their specific dynamic ranges.

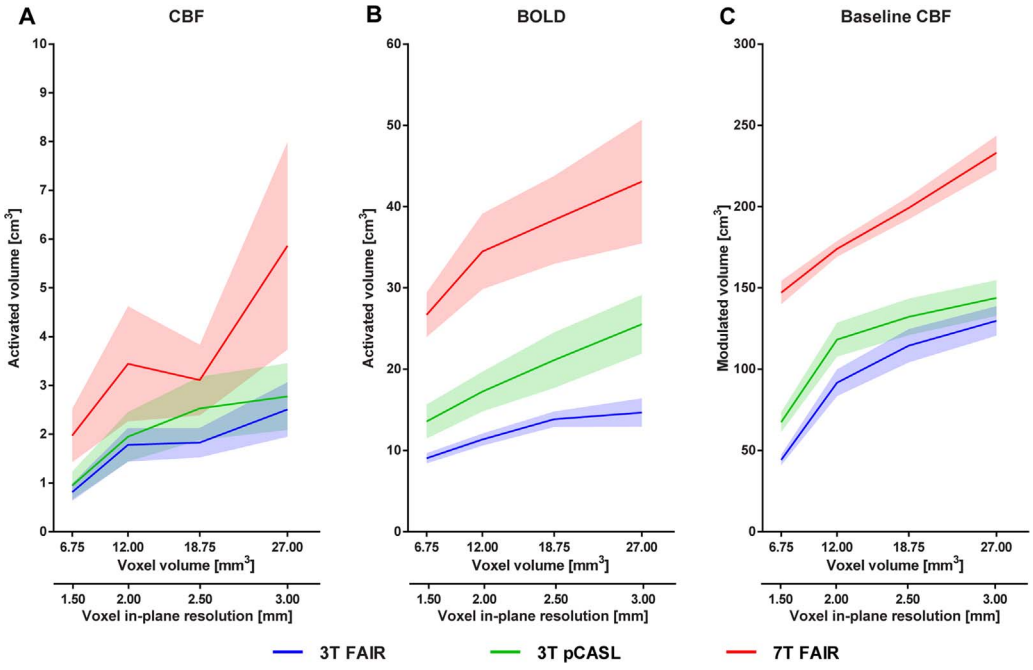

Fig. 6. Results of the full GLM ASL model. Plots A and B show the amount of volume detected as active by the CBF and BOLD predictors, respectively. Plot C shows the amount of GM volume whose time-course was significantly modulated according to the baseline CBF predictor. Lines and shades represent the mean and standard error across the subjects, respectively.

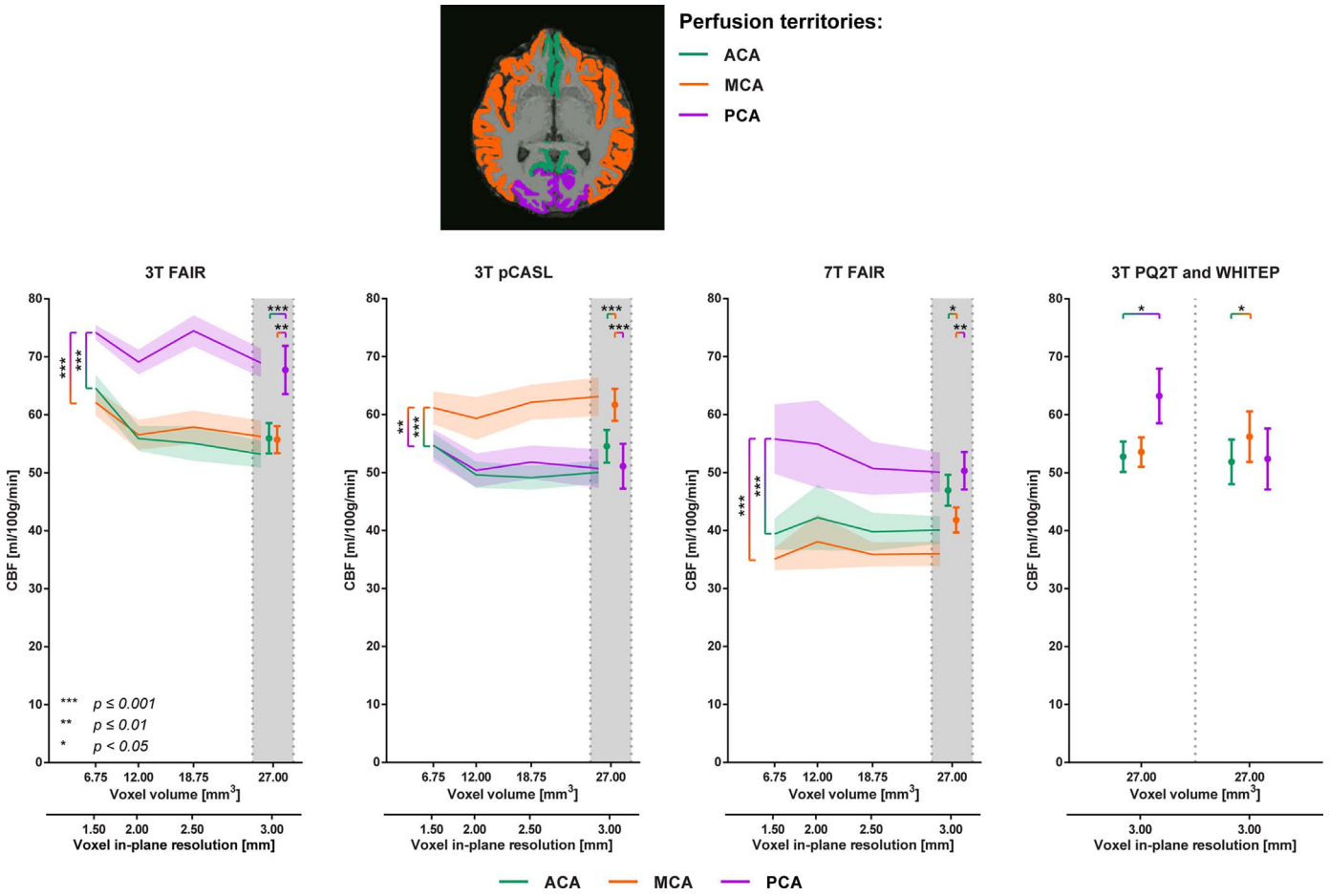

Fig. 7. Perfusion territory GM masks and CBF values. Anatomically-defined perfusion territories are shown (for a representative subject) in the image above the plots: green, orange, and purple masks correspond to the ACA, MCA and PCA territories. Territory-specific CBF values are shown as a function of voxel volume using the corresponding colors (continuous lines for Experiment 2 and circles for Experiment 1). Note that in this figure, masks and values were shown without differentiating between left and right part of each territory (i.e. contributions from the left and right part of each territory were averaged prior to the display).

The influence of magnetic field strength

The CBF and BOLD signal sensitivities across field strengths also depend on the receive coil array used. In particular, the parallel imaging performance is highly sensitive to the RF coil employed (Keil and Wald, 2013). It is worth mentioning that the way the receive array, parallel imaging and voxel size directly influence the CBF and BOLD sensitivities is through their effects on tSNR (Wald, 2012). Furthermore, the performance of a receive array with the same arrangement of the elements changes with the field strength due to the different RF wavelength employed (Wiesinger et al., 2004). In this study, coils with different number of elements were used at the two field strengths because of availability constraints. However, due to the use of 2D EPI, not all coil elements present in the receive array actually contribute to image formation. Thus, we do not expect significant differences when using coils with matching number of elements across field strengths. Therefore, the influence of the RF coils is considered here as an integral part of the field-strength effect on tSNR and parallel imaging performance.

We observed that 7 T ASL has higher perfusion tSNR than 3 T ASL for all resolutions and labeling schemes investigated when parallel imaging is used. Control tSNR, TE, bolus length and PLD are the key parameters that determine the perfusion tSNR. When using GRAPPA, the larger control tSNR at 7 T with respect to 3 T is the main source of improved perfusion tSNR at 7 T. In fact, the control tSNR can serve as a metric not only for the effect of field strength, but also for that of parallel imaging and spatial resolution. When parallel imaging is not applied, 7 T control tSNR (for 3 mm in-plane resolution) is lower than that of the 3 T approaches and the perfusion tSNR is also lower. Phantom measurement using the same sequences and parameters showed higher control tSNR at 7 T that at 3 T indicating that increased physiological noise at ultra-high field might explain the lower in vivo control tSNR without parallel imaging (data not shown). The higher perfusion tSNR at 7 T translates into significantly larger CNR (Fig. 4B), baseline CBF modulated volume and CBF activated volume (Fig. 6). It is worth pointing out the utilization of dielectric pads at 7 T may also increase the perfusion tSNR, especially in the areas supplied by the vertebral arteries. For more details about this we refer the reader to the Supplementary Material and Supplementary Fig. S3, in particular. Fig. 5 also illustrates the advantages of 7 T over 3 T for mapping the CBF functional response across the visual areas. These results point out that the image (control) SNR increase (when parallel imaging is used) rather than the longer T_1s at 7 T plays the decisive role for the advantages of 7 T ASL with respect to 3 T ASL. The observed 7 T benefits for functional BOLD mapping in terms of activation volume and extent are expected and have been reported numerous times (van der Zwaag et al., 2009; Donahue et al., 2011). The smaller portion of the brain significantly activated using CBF than using the BOLD signal is linked to their large difference in tSNR and CNR. Methods to decrease this disparity in CNR between the two by boosting CBF sensitivity or reducing the BOLD signal sensitivity, like background suppression or alternative readout approaches, are discussed below.

High-quality, high spatial resolution ASL is enabled by parallel imaging through reducing TE and shortening the readout duration to

increase the perfusion signal and reduce blurring and susceptibility artefacts. However, the undersampling used in parallel imaging leads to a tSNR decrease, especially in the center of the brain, where the g-factor penalty is largest. This can be observed well in Fig. 3, where the 3 T perfusion tSNRs using GRAPPA in the subcortical structures are lower across all resolutions in comparison to the non-accelerated 3 T and all 7 T images. Importantly, it is possible to observe that this effect is more pronounced for 3 T ASL than 7 T ASL. Measurements indicated that, for the acceleration factor used here, the g-factor was globally 3.8% (and locally up to 10%) smaller at 7 T than at 3 T (data not shown). Improved parallel imaging performance at 7 T has been demonstrated previously (Wiesinger et al., 2004; Keil and Wald, 2013) and could also partly contribute to the higher perfusion and control tSNR at 7 T observed here. It is important to note that the lower image SNR for a given voxel size when GRAPPA is used at 3 T with respect to the 7 T, is also accompanied with a smaller physiological noise.

Differences in absolute CBF values between 3 T and 7 T

Although perfusion quantification is typically not the main point of interest for functional CBF studies, quantification remains a major advantage of ASL compared to BOLD techniques. The obtained quantitative CBF values were largely independent of spatial resolution, parallel imaging, and labeling scheme, but a significantly reduced mean GM CBF at 7 T with respect to 3 T was found. This finding is in line with those from previous studies at UHF and can have several reasons (St Lawrence and Wang, 2005; Bause et al., 2016). First, labeling efficiency is a direct scaling factor for CBF and using a wrong (overestimated) value for it will lead to underestimation. Second, the temporal duration of the label for PASL sequences is another scaling factor that was assumed, whose overestimation would lead to lower CBF. Both factors may influence the CBF estimation as a function of field strength at the individual and/or group level, since they mainly depend on the B_1^+- and B_0-homogeneity in the labeling region. It is worth mentioning that the extent of the inversion (label) at 7 T is ultimately limited by the distribution of the local transmit coil B_1^+ profile with respect to the subject's vascular anatomy, and may be shorter than that achieved using the 3 T body transmit coil. Further, the field homogeneity at 7 T presumably remained lower than typical 3 T values, despite the application of dielectric pads and optimized inversion pulses. Substantial technical developments, such as parallel transmission techniques and dedicated labeling coils, might be necessary to achieve labeling performance similar to the current 3 T scanners. The third potential reason for the lower CBF at 7 T relates to the single-compartment model used for its calculation. St Lawrence and Wang demonstrated that, due to the T_2* differences between the capillary blood and tissue compartment, CBF at 7 T obtained with this model will be increasingly underestimated with increasing TE due to the drop in the capillary ASL signal (St Lawrence and Wang, 2005). In particular, for the 13 ms TE used here, the underestimation would amount to 10%, which is less than the difference between the 3 T and 7 T CBF, pointing to the possibility that the first two factors described above also play a role.

The effect of spatial resolution

The voxel size decrease is accompanied with a reduction in image (control) SNR and tSNR. The presence of physiological noise prevents improvements in image SNR to translate into commensurate increased tSNR. Increasing the spatial resolution reduces the physiological noise contribution to the time-series variance (Triantafyllou et al., 2011). Consequently, at high spatial resolution, the thermal noise begins dominating the temporal variance, and the relationship between tSNR and voxel volume becomes linear. For which imaging parameters this happens will depend on the field strength, receive coil, acceleration factor, reconstruction approach and echo time. Fig. 4 suggests that the slope of the control tSNR dependence on the voxel volume at 3 T might change between 1.5–2 mm and 2–3 mm in-plane resolution, potentially indicating a change between the thermal noise- and physiological noise-dominated regime. Another indication for this might be the larger tSNR loss between the aforementioned in-plane resolutions at 3 T than at 7 T. Furthermore, due to the decrease in perfusion and control tSNR with increasing spatial resolution, the CBF and BOLD activation volume and the baseline CBF modulated volume continuously decreased at both fields (Fig. 6).

There are two main effects that take place when the spatial resolution is increased – the image SNR and time-series tSNR decrease, while the partial voluming between WM, GM and CSF is reduced. The GM thickness across the brain varies between 2 and 4 mm, i.e. it is comparable to the voxel sizes employed in this study. Accordingly, significantly higher CBF at the 1.5 mm in-plane resolution compared to the other resolutions acquired was observed for 3 T FAIR and pCASL, but not for 7 T FAIR (Fig. 2B). This suggests that low perfusion tSNR and/or reduced partial voluming at high spatial resolutions at 3 T may be causing this. In particular, the acquisition of smaller voxels leads to increased mean GM CBF, due to the fact that partial voluming with both CSF and white matter decreases the GM voxel's perfusion estimate. The latter effect has been claimed to be one of the reasons for the quantitative discrepancies in CBF observed between ASL and PET (Donahue et al., 2006).

Dual-echo vs. single-echo ASL

The perfusion tSNR, perfusion CNR and CBF activated volumes all decrease with increasing TE irrespective of the field strength (see Supplementary Figs. S1 and S2). In contrast, the BOLD signal has highest CNR at an echo time equal to the local T_2* of tissue. Thus, the TE of the acquisition has a key influence on the CBF and BOLD sensitivities and should be carefully chosen. In the case of a single-echo approach, a compromise between CBF and BOLD sensitivities typically needs to be made. Dual-echo will be beneficial when the second TE is close to the optimal TE for BOLD imaging, while the first TE is as short as possible. Indeed, 3 T control CNR and BOLD activated volume significantly increased for the second TE (independently of labeling scheme and spatial resolution), while the 7 T BOLD activated volume obtained using the second TE was smaller than the one obtained at the first TE across all resolutions (Supplementary Fig. S2B). This latter result can be explained by the significantly shorter T_2* at 7 T than at 3 T, and single-echo ASL should be the preferred option at 7 T, especially in the case of high resolution. In general, dual-echo will be a viable option at 7 T only if low resolution is sufficient, since then the readouts and both TEs can be kept short through the use of partial Fourier or/and parallel imaging. In contrast, dual-echo is the preferred option at 3 T across a range of resolutions because the tradeoffs of a single-echo affect negatively both the CBF and BOLD sensitivities.

The influence of labeling scheme

Most functional ASL experiments to date have used PASL, but the recent widespread availability of pCASL has changed this trend, especially for pharmacological and calibrated fMRI studies, where rapid temporal changes are uncommon. PCASL has demonstrated higher within-session reproducibility and perfusion tSNR than PASL (Chen et al., 2011). The latter result is also confirmed by our findings. As mentioned above, pCASL allows longer labeling durations, albeit with lower inversion efficiency than PASL schemes. One drawback of pCASL compared to PASL is the lower temporal resolution due to the need for sufficient PLD before the data acquisition to avoid vascular artefacts. Moreover, the arterial transit times in PASL schemes across the brain are typically shorter than those of pCASL (Chen et al., 2012). In cases when short TRs are required, as in a functional study, a compromise between labeling duration and PLD needs to be found.

The tradeoff chosen here is to keep both approximately equal, in order to maximize the labeling duration and therefore perfusion tSNR. Our results suggest that a PLD of about 1 s may still be adequate for the brain regions within the MCA perfusion territory, and potentially for the ones supplied by the ACA, but is clearly too short for those perfused by the PCA. The findings are in agreement with pCASL arterial transit time measurements of around 1 s for MCA and ACA and 1.5 s for PCA (Chen et al., 2012; Qin et al., 2014). Figs. 2A and 3 show perfusion signal inhomogeneities with 'hot spots' of high signal and neighboring dark voxels within the GM belonging to the posterior perfusion territory. This is in contrast to the smooth GM delineation of the PASL and WHITEP images in the same areas. It is worth noting that we do not expect any significant differences in the results obtained with our WHITEP implementation and a pCASL protocol with a 1.8 s PLD, as recommended in the white paper. Fig. 7 depicts the perfusion territories' CBF differences across the approaches tested. PCASL shows significantly higher CBF in the MCA than both the ACA and PCA perfusion territories. In the WHITEP case, T_1-decay may cause the decreased CBF in the MCA territory, whereas the completed label delivery would increase that of PCA, and only the significant difference between MCA and ACA remains. These results underscore that a PLD of 1.5 s or longer is required to ensure artefact-free perfusion images for pCASL across the entire brain, albeit increasing the current TR for pCASL by at least 500 ms. It is worth mentioning that non-uniform labeling efficiency between carotid and vertebral arteries and/or flow velocity sensitivity may also influence the perfusion territories' CBF distribution obtained by pCASL. Despite the SNR benefits of pCASL at 3 T, its practical implementation at 7 T is hindered by its high power deposition and sensitivity to field inhomogeneities.

Fig. 7 indicates that the PASL schemes result in significantly higher CBF in the PCA perfusion territory. Several previous studies (Cavusoglu et al., 2009; Wang et al., 2011; Qin et al., 2014) measured higher CBF in the PCA compared to the MCA and ACA territories, while other PASL studies did not (Chen et al., 2011). Our findings may be linked to the different flow velocities and therefore transit times of the brain-feeding arteries (Yazici et al., 2005; Chen et al., 2012; Guo et al., 2016). The velocity in the vertebral arteries that supply the posterior areas is typically lower than in the carotids, which deliver blood to the MCA and ACA territories, causing the PCA bolus temporal width to be longer (even for a uniform inversion slab thickness) and be delivered later. In addition, the spatial fidelity of the inversion slab may be compromised due to B_1^+- and B_0-inhomogenities, especially at 7 T, also leading to non-uniform CBF distribution across vascular territories. The QUIPSS and Q2TIPS saturation pulses are typically applied to control the label duration across all feeding vessels, but B_1^+-inhomogeneities may confound their performance resulting in atypical CBF distributions. All the aforementioned factors may lead to differences between the bolus widths across vascular territories in PASL and thereby between their CBF. Nevertheless, for the same temporal bolus width, stronger perfusion-weighted signal and higher CBF in the PCA perfusion territory may also result from a reduced T_1-decay compared to the MCA and ACA, due to the longer duration the label resides in the vasculature. A wedge-shaped slab-selective inversion pulse, recently proposed by (Guo et al., 2016), may achieve equal bolus duration across the perfusion territories without additional saturation pulses. It is worth noting that the CBF differences between perfusion territories among labeling schemes reported here should be considered when comparing measurements across ASL approaches, as they constitute a potential confound for baseline and stimulus-induced quantitative CBF values.

The significantly higher perfusion tSNR of pCASL leads to larger CBF activation volume than 3 T FAIR, albeit the difference was not statistically significant. It is possible that the higher mean perfusion tSNR for pCASL than PASL, despite the relatively short labeling time, is also related to the insufficient PLD. In comparison, the lack of significant difference in control tSNR between 3 T FAIR and pCASL makes the significantly larger BOLD activation volume of the latter appear puzzling. We hypothesize that the disparity in BOLD sensitivity is caused by the difference in longitudinal magnetization between the two, due to the application of presaturation and inversion pulses in FAIR – an effect similar to the application of background suppression.

The effect of background suppression and readout scheme

The omission of background suppression and the use of 2D GE EPI for all the techniques investigated here were dictated by the requirement for short TR, which is incompatible with the utilization of spin-echo approaches due to the SAR restrictions at 7 T. Background suppression substantially decreases the tissue signal and physiological noise associated with it and therefore improves the perfusion SNR. However, since the BOLD sensitivity depends also on the background tissue signal, it is reduced as well. Background suppression is ideally combined with a 3D readout but is also useful in 2D EPI. The key disadvantage, and the main reason for its omission in this study, is its high power deposition making it incompatible with the stringent 7 T SAR limits.

The 2D EPI readout was chosen for this functional ASL comparison (and in many other studies), mainly because of its widespread availability, as well as its temporal efficiency and robustness to motion compared to other alternatives, such as segmented 3D SE readouts. Single-shot 3D SE PASL approaches can achieve temporal resolutions similar to the ones used here and may result in improved perfusion measurements (Vidorreta et al., 2013) albeit with reduced BOLD sensitivity. 3D EPI readouts (Poser et al., 2010) are well-suited for simultaneous CBF and BOLD measurements (Gai et al., 2011), for combination with background suppression, and have been successfully implemented at 7 T (Hall et al., 2010; Ivanov et al., 2016) because of their low power deposition. 3D EPI outperforms 2D EPI in the thermal noise-dominated regime of high spatial resolutions, but they are comparable in the physiological noise-dominated regime (Poser et al., 2010; Huber et al., 2017). In summary, even though 2D EPI is not the ideal readout for all perfusion applications it is well-suited for high temporal resolution, simultaneous functional CBF and BOLD mapping, especially in the low spatial resolution regime. The simultaneous multi-slice 2D EPI significantly increases the brain coverage with only a slight SNR penalty (Ivanov et al., in press). Sensitivity improvements with comparable temporal resolution, particularly at UHF, may be obtained by the utilization of 3D EPI with background suppression and/or 3D EPI combined with the double acquisition background suppressed (DABS) FAIR (Wesolowski et al., 2009). At 3 T, the combination of a background-suppressed single-shot 3D GRASE readout for the CBF and 2D EPI for BOLD imaging has shown great promise (Fernandez-Seara et al., 2016), but with less than half the temporal resolution achieved here.

Conclusions

The benefits and challenges of performing ASL studies at 7 T compared to 3 T were explored. To adequately compare the signal quality and CBF and BOLD signal functional sensitivity, the field strength effect was thoroughly investigated by taking into account also the influence of other acquisition factors, such as parallel imaging, spatial resolution, echo time and labeling scheme. It is demonstrated that high spatial and temporal resolution functional CBF and BOLD imaging can be achieved using the presented single-echo 7 T PASL scheme. Its superiority over 3 T approaches stems from the higher BOLD sensitivity and higher image SNR at UHF. At 3 T, dual-echo pCASL without acceleration delivers optimal perfusion sensitivity for low spatial and temporal resolution applications.

Acknowledgements

The research was supported by Maastricht University and the Netherlands Organization for Scientific Research NWO: VIDI 452-11-002 to Kâmil Uludağ. We would like to thank Dr. Laurentius Huber for the implementation and validation of the tr-FOCI RF pulse and Sriranga Kashyap for help with the stimulus setup. The authors are indebted to Professor Dr. Andrew Webb for providing the dielectric pads used in this study.

Appendix A. Supporting information

Supplementary data associated with this article can be found in the online version at doi:10.1016/j.neuroimage.2017.05.038.

References

Alsop, D.C., Detre, J.A., Golay, X., Gunther, M., Hendrikse, J., Hernandez-Garcia, L., Lu, H., MacIntosh, B.J., Parkes, L.M., Smits, M., van Osch, M.J., Wang, D.J., Wong, E.C., Zaharchuk, G., 2015. Recommended implementation of arterial spin-labeled perfusion MRI for clinical applications: a consensus of the ISMRM perfusion study group and the European consortium for ASL in dementia. Magn. Reson. Med. 73, 102–116.

Andersson, J.L., Skare, S., Ashburner, J., 2003. How to correct susceptibility distortions in spin-echo echo-planar images: application to diffusion tensor imaging. Neuroimage 20, 870–888.

Bause, J., Ehses, P., Mirkes, C., Shajan, G., Scheffler, K., Pohmann, R., 2016. Quantitative and functional pulsed arterial spin labeling in the human brain at 9.4 T. Magn. Reson. Med. 75, 1054–1063.

Bulte, D.P., Kelly, M., Germuska, M., Xie, J., Chappell, M.A., Okell, T.W., Bright, M.G., Jezzard, P., 2012. Quantitative measurement of cerebral physiology using respiratory-calibrated MRI. Neuroimage 60, 582–591.

Buxton, R.B., Griffeth, V.E., Simon, A.B., Moradi, F., Shmuel, A., 2014. Variability of the coupling of blood flow and oxygen metabolism responses in the brain: a problem for interpreting BOLD studies but potentially a new window on the underlying neural activity. Front. Neurosci. 8, 139.

Cavusoglu, M., Bartels, A., Yesilyurt, B., Uludag, K., 2012. Retinotopic maps and hemodynamic delays in the human visual cortex measured using arterial spin labeling. Neuroimage 59, 4044–4054.

Cavusoglu, M., Pfeuffer, J., Ugurbil, K., Uludag, K., 2009. Comparison of pulsed arterial spin labeling encoding schemes and absolute perfusion quantification. Magn. Reson. Imaging 27, 1039–1045.

Chen, Y., Wang, D.J., Detre, J.A., 2011. Test-retest reliability of arterial spin labeling with common labeling strategies. J. Magn. Reson. Imaging 33, 940–949.

Chen, Y., Wang, D.J., Detre, J.A., 2012. Comparison of arterial transit times estimated using arterial spin labeling. Magma 25, 135–144.

Dai, W., Garcia, D., de Bazelaire, C., Alsop, D.C., 2008. Continuous flow-driven inversion for arterial spin labeling using pulsed radio frequency and gradient fields. Magn. Reson. Med. 60, 1488–1497.

de Zwart, J.A., van Gelderen, P., Golay, X., Ikonomidou, V.N., Duyn, J.H., 2006. Accelerated parallel imaging for functional imaging of the human brain. NMR Biomed. 19, 342–351.

Desikan, R.S., Segonne, F., Fischl, B., Quinn, B.T., Dickerson, B.C., Blacker, D., Buckner, R.L., Dale, A.M., Maguire, R.P., Hyman, B.T., Albert, M.S., Killiany, R.J., 2006. An automated labeling system for subdividing the human cerebral cortex on MRI scans into gyral based regions of interest. Neuroimage 31, 968–980.

Destrieux, C., Fischl, B., Dale, A., Halgren, E., 2010. Automatic parcellation of human cortical gyri and sulci using standard anatomical nomenclature. Neuroimage 53, 1–15.

Detre, J.A., Alsop, D.C., Vives, L.R., Maccotta, L., Teener, J.W., Raps, E.C., 1998. Noninvasive MRI evaluation of cerebral blood flow in cerebrovascular disease. Neurology 50, 633–641.

Detre, J.A., Leigh, J.S., Williams, D.S., Koretsky, A.P., 1992. Perfusion imaging. Magn. Reson. Med. 23, 37–45.

Detre, J.A., Wang, J., 2002. Technical aspects and utility of fMRI using BOLD and ASL. Clin. Neurophysiol. : Off. J. Int. Fed. Clin. Neurophysiol. 113, 621–634.

Dobre, M.C., Ugurbil, K., Marjanska, M., 2007. Determination of blood longitudinal relaxation time (T1) at high magnetic field strengths. Magn. Reson. Imaging 25, 733–735.

Donahue, M.J., Hoogduin, H., van Zijl, P.C., Jezzard, P., Luijten, P.R., Hendrikse, J., 2011. Blood oxygenation level-dependent (BOLD) total and extravascular signal changes and DeltaR2* in human visual cortex at 1.5, 3.0 and 7.0 T. NMR Biomed. 24, 25–34.

Donahue, M.J., Lu, H., Jones, C.K., Pekar, J.J., van Zijl, P.C., 2006. An account of the discrepancy between MRI and PET cerebral blood flow measures. A high-field MRI investigation. NMR Biomed. 19, 1043–1054.

Duong, T.Q., Kim, D.S., Ugurbil, K., Kim, S.G., 2001. Localized cerebral blood flow response at submillimeter columnar resolution. Proc. Natl. Acad. Sci. USA 98, 10904–10909.

Duong, T.Q., Yacoub, E., Adriany, G., Hu, X., Ugurbil, K., Vaughan, J.T., Merkle, H., Kim, S.G., 2002. High-resolution, spin-echo BOLD, and CBF fMRI at 4 and 7 T. Magn. Reson. Med. 48, 589–593.

Farzaneh, F., Riederer, S.J., Pelc, N.J., 1990. Analysis of T2 limitations and off-resonance effects on spatial resolution and artifacts in echo-planar imaging. Magn. Reson. Med. 14, 123–139.

Fernandez-Seara, M.A., Rodgers, Z.B., Englund, E.K., Wehrli, F.W., 2016. Calibrated bold fMRI with an optimized ASL-BOLD dual-acquisition sequence. Neuroimage 142, 474–482.

Gai, N.D., Talagala, S.L., Butman, J.A., 2011. Whole-brain cerebral blood flow mapping using 3D echo planar imaging and pulsed arterial tagging. J. Magn. Reson. Imaging 33, 287–295.

Gardener, A.G., Gowland, P.A., Francis, S.T., 2009. Implementation of quantitative perfusion imaging using pulsed arterial spin labeling at ultra-high field. Magn. Reson. Med. 61, 874–882.

Gardener, A.G., Jezzard, P., 2015. Investigating white matter perfusion using optimal sampling strategy arterial spin labeling at 7 Tesla. Magn. Reson. Med. 73, 2243–2248.

Ghariq, E., Chappell, M.A., Schmid, S., Teeuwisse, W.M., van Osch, M.J., 2014. Effects of background suppression on the sensitivity of dual-echo arterial spin labeling MRI for BOLD and CBF signal changes. Neuroimage 103, 316–322.

Ghariq, E., Teeuwisse, W.M., Webb, A.G., van Osch, M.J., 2012. Feasibility of pseudocontinuous arterial spin labeling at 7 T with whole-brain coverage. Magma 25, 83–93.

Griswold, M.A., Jakob, P.M., Heidemann, R.M., Nittka, M., Jellus, V., Wang, J., Kiefer, B., Haase, A., 2002. Generalized autocalibrating partially parallel acquisitions (GRAPPA). Magn. Reson. Med. 47, 1202–1210.

Guo, J., Buxton, R.B., Wong, E.C., 2016. Wedge-shaped slice-selective adiabatic inversion pulse for controlling temporal width of bolus in pulsed arterial spin labeling. Magn. Reson. Med. 76, 838–847.

Hall E.L., Gowland P., Francis S.T., 2010. 3D-EPI ASL at Ultra High Field. In: Joint Annual Meeting ISMRM-ESMRMB. Stockholm, Sweden, p. 517.

Havlicek, M., Roebroeck, A., Friston, K., Gardumi, A., Ivanov, D., Uludag, K., 2015. Physiologically informed dynamic causal modeling of fMRI data. Neuroimage 122, 355–372.

Hernandez-Garcia, L., Jahanian, H., Rowe, D.B., 2010. Quantitative analysis of arterial spin labeling FMRI data using a general linear model. Magn. Reson. Imaging 28, 919–927.

Huber, L., Ivanov, D., Handwerker, D.A., Marrett, S., Guidi, M., Uludag, K., Bandettini, P., Poser, B.A., 2017. Techniques for blood volume fMRI with VASO: from low-resolution mapping towards sub-millimeter layer-dependent applications. Neuroimage. http://dx.doi.org/10.1016/j.neuroimage.2016.11.039, (In Press).

Hurley, A.C., Al-Radaideh, A., Bai, L., Aickelin, U., Coxon, R., Glover, P., Gowland, P.A., 2010. Tailored RF pulse for magnetization inversion at ultrahigh field. Magn. Reson. Med. 63, 51–58.

Ivanov, D., Poser, B.A., Huber, L., Pfeuffer, J., Uludag, K., 2017a. Optimization of simultaneous multislice EPI for concurrent functional perfusion and BOLD signal measurements at 7 T. Magn. Reson. Med.. http://dx.doi.org/10.1002/mrm.26351, (In Press).

Ivanov, D., Poser, B.A., Kashyap, S. Gardumi, A., Huber, L., Uludag, K., 2016. Sub-millimeter human brain perfusion maps using arterial spin labelling at 3 and 7 T. In: ISMRM Workshop on Ultra High Field MRI. p. 14.

Jenkinson, M., Bannister, P., Brady, M., Smith, S., 2002. Improved optimization for the robust and accurate linear registration and motion correction of brain images. Neuroimage 17, 825–841.

Keil, B., Wald, L.L., 2013. Massively parallel MRI detector arrays. J. Magn. Reson. 229, 75–89.

Krieger, S.N., Gauthier, C.J., Ivanov, D., Huber, L., Roggenhofer, E., Sehm, B., Turner, R., Egan, G.F., 2014. Regional reproducibility of calibrated BOLD functional MRI: implications for the study of cognition and plasticity. Neuroimage 101, 8–20.

Lu, H., Clingman, C., Golay, X., van Zijl, P.C., 2004. Determining the longitudinal relaxation time (T1) of blood at 3.0 T. Magn. Reson. Med. 52, 679–682.

Luh, W.M., Talagala, S.L., Li, T.Q., Bandettini, P.A., 2013. Pseudo-continuous arterial spin labeling at 7 T for human brain: estimation and correction for off-resonance effects using a Prescan. Magn. Reson. Med. 69, 402–410.

Luh, W.M., Wong, E.C., Bandettini, P.A., Hyde, J.S., 1999. QUIPSS II with thin-slice TI1 periodic saturation: a method for improving accuracy of quantitative perfusion imaging using pulsed arterial spin labeling. Magn. Reson. Med. 41, 1246–1254.

Luh, W.M., Wong, E.C., Bandettini, P.A., Ward, B.D., Hyde, J.S., 2000. Comparison of simultaneously measured perfusion and BOLD signal increases during brain activation with T(1)-based tissue identification. Magn. Reson. Med. 44, 137–143.

Mumford, J.A., Hernandez-Garcia, L., Lee, G.R., Nichols, T.E., 2006. Estimation efficiency and statistical power in arterial spin labeling fMRI. Neuroimage 33, 103–114.

Norris, D.G., 2003. High field human imaging. J. Magn. Reson. Imaging 18, 519–529.

Pfeuffer, J., Adriany, G., Shmuel, A., Yacoub, E., Van De Moortele, P.F., Hu, X., Ugurbil, K., 2002. Perfusion-based high-resolution functional imaging in the human brain at 7 T. Magn. Reson. Med. 47, 903–911.

Pohmann, R., Speck, O., Scheffler, K., 2016. Signal-to-noise ratio and MR tissue parameters in human brain imaging at 3, 7, and 9.4 T using current receive coil arrays. Magn. Reson. Med. 75, 801–809.

Polimeni, J.R., Bhat, H., Witzel, T., Benner, T., Feiweier, T., Inati, S.J., Renvall, V., Heberlein, K., Wald, L.L., 2016. Reducing sensitivity losses due to respiration and motion in accelerated echo planar imaging by reordering the autocalibration data acquisition. Magn. Reson. Med. 75, 665–679.

Poser, B.A., Koopmans, P.J., Witzel, T., Wald, L.L., Barth, M., 2010. Three dimensional echo-planar imaging at 7 T. Neuroimage 51, 261–266.

Qin, Q., Huang, A.J., Hua, J., Desmond, J.E., Stevens, R.D., van Zijl, P.C., 2014. Three-dimensional whole-brain perfusion quantification using pseudo-continuous arterial spin labeling MRI at multiple post-labeling delays: accounting for both arterial transit time and impulse response function. NMR Biomed. 27, 116–128.
Reuter, M., Rosas, H.D., Fischl, B., 2010. Highly accurate inverse consistent registration: a robust approach. Neuroimage 53, 1181–1196.
Rooney, W.D., Johnson, G., Li, X., Cohen, E.R., Kim, S.G., Ugurbil, K., Springer, C.S., Jr., 2007. Magnetic field and tissue dependencies of human brain longitudinal 1H2O relaxation in vivo. Magn. Reson. Med. 57, 308–318.
Smith, S.M., Jenkinson, M., Woolrich, M.W., Beckmann, C.F., Behrens, T.E., Johansen-Berg, H., Bannister, P.R., De Luca, M., Drobnjak, I., Flitney, D.E., Niazy, R.K., Saunders, J., Vickers, J., Zhang, Y., De Stefano, N., Brady, J.M., Matthews, P.M., 2004. Advances in functional and structural MR image analysis and implementation as FSL. Neuroimage 23 (Suppl. 1), S208–219.
St Lawrence, K.S., Wang, J., 2005. Effects of the apparent transverse relaxation time on cerebral blood flow measurements obtained by arterial spin labeling. Magn. Reson. Med. 53, 425–433.
Tatu, L., Moulin, T., Vuillier, F., Bogousslavsky, J., 2012. Arterial territories of the human brain. Front. Neurol. Neurosci. 30, 99–110.
Teeuwisse, W.M., Brink, W.M., Webb, A.G., 2012. Quantitative assessment of the effects of high-permittivity pads in 7 Tesla MRI of the brain. Magn. Reson. Med. 67, 1285–1293.
Teeuwisse, W.M., Webb, A.G., van Osch, M.J.R., 2010. Arterial spin labeling at ultra-high field: all that glitters is not gold. Int. J. Imag. Syst. Technol. 20, 62–70.
Tjandra, T., Brooks, J.C., Figueiredo, P., Wise, R., Matthews, P.M., Tracey, I., 2005. Quantitative assessment of the reproducibility of functional activation measured with BOLD and MR perfusion imaging: implications for clinical trial design. Neuroimage 27, 393–401.
Triantafyllou, C., Polimeni, J.R., Wald, L.L., 2011. Physiological noise and signal-to-noise ratio in fMRI with multi-channel array coils. Neuroimage 55, 597–606.
Uludag, K., Muller-Bierl, B., Ugurbil, K., 2009. An integrative model for neuronal activity-induced signal changes for gradient and spin echo functional imaging. Neuroimage 48, 150–165.
Van de Moortele, P.F., Auerbach, E.J., Olman, C., Yacoub, E., Ugurbil, K., Moeller, S., 2009. T1 weighted brain images at 7 Tesla unbiased for Proton Density, T2* contrast and RF coil receive B1 sensitivity with simultaneous vessel visualization. Neuroimage 46, 432–446.
van der Zwaag, W., Francis, S., Head, K., Peters, A., Gowland, P., Morris, P., Bowtell, R., 2009. fMRI at 1.5, 3 and 7 T: characterising BOLD signal changes. Neuroimage 47, 1425–1434.
Vidorreta, M., Wang, Z., Rodriguez, I., Pastor, M.A., Detre, J.A., Fernandez-Seara, M.A., 2013. Comparison of 2D and 3D single-shot ASL perfusion fMRI sequences. Neuroimage 66, 662–671.
Wald, L.L., 2012. The future of acquisition speed, coverage, sensitivity, and resolution. Neuroimage 62, 1221–1229.
Wang, Y., Moeller, S., Li, X., Vu, A.T., Krasileva, K., Ugurbil, K., Yacoub, E., Wang, D.J., 2015a. Simultaneous multi-slice Turbo-FLASH imaging with CAIPIRINHA for whole brain distortion-free pseudo-continuous arterial spin labeling at 3 and 7 T. Neuroimage 113, 279–288.
Wang, Y., Moeller, S., Li, X., Vu, A.T., Krasileva, K., Ugurbil, K., Yacoub, E., Wang, D.J., 2015b. Simultaneous multi-slice Turbo-FLASH imaging with CAIPIRINHA for whole brain distortion-free pseudo-continuous arterial spin labeling at 3 and 7 T. Neuroimage 113, 279–288.
Wang, Y., Saykin, A.J., Pfeuffer, J., Lin, C., Mosier, K.M., Shen, L., Kim, S., Hutchins, G.D., 2011. Regional reproducibility of pulsed arterial spin labeling perfusion imaging at 3 T. Neuroimage 54, 1188–1195.
Welvaert, M., Rosseel, Y., 2013. On the definition of signal-to-noise ratio and contrast-to-noise ratio for FMRI data. PLoS One 8, e77089.
Wesolowski, R., Gowland, P., Francis, S.T., 2009. Double Acquisition Background Suppressed (DABS) FAIR at 3 T and 7 T: advantages for simultaneous BOLD and CBF acquisition. In: Proceedings of the 17th Annual Meeting of the ISMRM, p. 1526.
Wiesinger, F., Van de Moortele, P.F., Adriany, G., De Zanche, N., Ugurbil, K., Pruessmann, K.P., 2004. Parallel imaging performance as a function of field strength–an experimental investigation using electrodynamic scaling. Magn. Reson. Med. 52, 953–964.
Williams, D.S., Detre, J.A., Leigh, J.S., Koretsky, A.P., 1992. Magnetic resonance imaging of perfusion using spin inversion of arterial water. Proc. Natl. Acad. Sci. USA 89, 212–216.
Wong, E.C., Buxton, R.B., Frank, L.R., 1997. Implementation of quantitative perfusion imaging techniques for functional brain mapping using pulsed arterial spin labeling. NMR Biomed. 10, 237–249.
Wong, E.C., Buxton, R.B., Frank, L.R., 1998. Quantitative imaging of perfusion using a single subtraction (QUIPSS and QUIPSS II). Magn. Reson. Med. 39, 702–708.
Wright, P.J., Mougin, O.E., Totman, J.J., Peters, A.M., Brookes, M.J., Coxon, R., Morris, P.E., Clemence, M., Francis, S.T., Bowtell, R.W., Gowland, P.A., 2008. Water proton T1 measurements in brain tissue at 7, 3, and 1.5 T using IR-EPI, IR-TSE, and MPRAGE: results and optimization. Magma 21, 121–130.
Wu, W.C., Fernandez-Seara, M., Detre, J.A., Wehrli, F.W., Wang, J., 2007. A theoretical and experimental investigation of the tagging efficiency of pseudocontinuous arterial spin labeling. Magn. Reson. Med. 58, 1020–1027.
Yazici, B., Erdogmus, B., Tugay, A., 2005. Cerebral blood flow measurements of the extracranial carotid and vertebral arteries with Doppler ultrasonography in healthy adults. Diagn. Interv. Radiol. 11, 195–198.
Ye, F.Q., Frank, J.A., Weinberger, D.R., McLaughlin, A.C., 2000. Noise reduction in 3D perfusion imaging by attenuating the static signal in arterial spin tagging (ASSIST). Magn. Reson. Med. 44, 92–100.
Zhang, X., Petersen, E.T., Ghariq, E., De Vis, J.B., Webb, A.G., Teeuwisse, W.M., Hendrikse, J., van Osch, M.J., 2013. In vivo blood T(1) measurements at 1.5 T, 3 T, and 7 T. Magn. Reson. Med. 70, 1082–1086.
Zimmer, F., O'Brien, K., Bollmann, S., Pfeuffer, J., Heberlein, K., Barth, M., 2016. Pulsed arterial spin labelling at ultra-high field with a B1(+) -optimised adiabatic labelling pulse. Magma 29, 463–473.
Zuo, Z., Wang, R., Zhuo, Y., Xue, R., St Lawrence, K.S., Wang, D.J., 2013. Turbo-FLASH based arterial spin labeled perfusion MRI at 7 T. PLoS One 8, e66612.